Sol gel combustion derived monticellite bioceramic powders for apatite formation ability evaluation

Sol Gel Combustion Derived Monticellite Bioceramic Powders for Apatite Formation Ability Evaluation

Sivasankar Koppala[1*], Renita Mishal D Souza[2], Poornima Sivanandam[2], Sai Kumar Tammina[4], Kangqiang Li[3*], Quan Chen[3], Lei Xu[3*], Ramdas Balan[5], Sasikumar Swamiappan[2*]

[1]Panjin Institute of Industrial Technology, Dalian University of Technology, Panjin 124221, Liaoning, China

[2]Department of Chemistry, School of Advanced Sciences, VIT University, Vellore 632014, India

[3]Key Laboratory of Unconventional Metallurgy, Ministry of Education, Faculty of Metallurgical and Energy Engineering, Kunming University of Science and Technology, Kunming 650093, PR China

[4]Faculty of Environmental Science and Engineering, Kunming University of Science and Technology, Yunnan Province 650500, China

[5]Centre of Excellence in Materials Science, Department of Physics, CMR Institute of Technology, Bangalore 560037, Karnataka, India

*Corresponding Authors: pepsiva9@gmail.com (Sivasankar Koppala), ssasikumar@vit.ac.in (Sasikumar Swamiappan)

ABSTRACT

Sol-gel combustion method was employed for the synthesis of monticellite ($CaMgSiO_4$) ceramic powders using various fuels. Citric acid, succinic acid, tartaric acid, sucrose, urea, glycine, and L-alanine were used as fuels. Influence of calcination temperature on the phase evolution was

investigated. Prepared monticellite powders were characterized using powder-XRD, FT-IR, and DLS techniques. XRD pattern reveals that the L-alanine is a suitable fuel among all the fuels studied and confirms the formation of pure monticellite. FT-IR spectra confirm the presence of characteristic functional groups associated with monticellite. DLS measurements show the particle size of the monticellite powders. Finally, Apatite formation ability studies were carried out by immersing the monticellite and monticellite-polymer (chitosan/chitin) composites in the SBF solution. Pure monticellite shows higher bioactivity than the composites and its surface analysis (SEM and EDS) reveals the deposition of spherical hydroxyapatite particles.

KEYWORDS: Sol-Gel, Combustion, Fuel, Monticellite, Bioactivity, Hydroxyapatite

1. INTRODUCTION

Calcium magnesium silicates have potential biomedical, wear resistance, thermo-mechanical, ceramic coating and luminescent applications in the field of material science. Calcium magnesium silicate CaO-MgO-SiO_2 ternary system on crystallization exists in different phases such as monticellite ($CaMgSiO_4$), diopside ($CaMgSi_2O_6$), akermanite ($Ca_2MgSi_2O_7$), merwinite ($Ca_3MgSi_2O_8$), bredigite ($Ca_7MgSi_4O_{16}$), serendibite ($CaMg_3Si_3O_{10}$)) and tremolite ($Ca_2Mg_5Si_8O_{24}$) [1-5]. Among all, monticellite gains more research attention due to the salient features of the crystal structure. It is a naturally occurring mineral form during metamorphism of siliceous dolostones and named after Italian mineralogist Teodoro Monticelli. The first crystal structure reported by Bragg and Brown (1926) and subsequently refined by Brown (1970). Monticellite has an olivine-type crystal structure that exists in the orthorhombic crystal system with the space group Pmnb [6-8].

Considering the biomedical applications of monticellite, the first biomedical applications of monticellite ceramics reported in the year 2008. Monticellite possesses excellent bending strength (159.7 MPa), fracture toughness (1.63 MPa $m^{1/2}$) and Young's modulus (51 GPa). The coefficient of thermal expansion (10.76 $x10^{-6}$ $^0C^{-1}$) is close to that of Ti-6Al-4V alloy (10.03 $x10^{-6}$ $^0C^{-1}$). Monticellite induces the formation of bone-like apatite in physiological solutions as well as promotes osteoblasts cell growth and proliferation [9].

Various synthetic methods used in the past for the preparation of ceramic materials [10-13]. Especially, monticellite prepared by the solid-state method, sol-gel method and floating zone method, which require either higher calcination temperatures or special reduced atmospheric conditions [9, 14,

15]. Hence, it is worth attempting to prepare monticellite by a sol-gel combustion method, which doesn't require a special atmosphere or high calcination temperatures [16, 17]. As the material and its composites not explored, it is interesting to investigate the bioactivity properties in in-vitro conditions, which may be helpful in identifying monticellite as a biomedical material.

2. EXPERIMENTAL WORK

2.1 Materials

In the present investigation, the materials/chemicals were procured from commercial sources and used as such without further purification. The materials/chemicals used in the experiments are Calcium nitrate tetrahydrate (98.0%, Pure, SDFCL), magnesium nitrate hexahydrate (99.0 %, Qualigens), tetra ethyl ortho silicate (98.0%, Acros organics), nitric acid 1.42 (69.0 - 71.0 %, AR, SDFCL), citric acid anhydrous (99.5-101%, AR, SDFCL), succinic acid (99 %, Qualigens), Tartaric acid, sucrose (99.5%, AR, SDFCL), urea (99 %, Himedia), Glycine, L-alanine (99%, CHR, SDFCL), sodium chloride (99.9 %, AR, SDFCL,), sodium bicarbonate (99 %, LR, Nice chemicals), potassium chloride (99.5 %, AR, SDFCL), potassium hydrogen phosphate trihydrate (SDFCL), magnesium chloride hexahydrate (98-100.5 %, Qualigens), hydrochloric acid (35.4 % (1.18), AR, SDFCL), calcium chloride (90 %, LR, SDFCL), sodium sulphate (99.5 %, AR, SDFCL), Tris buffer (99.8 %, AR, SDFCL), chitin (Himedia), and chitosan (Sigma-Aldrich). Lattice parameters were calculated using powder X software.

2.2 Sol-Gel Combustion Synthesis

Sol-gel combustion method [16, 17] employed for the synthesis of monticellite in the pure phase. As shown in **Fig. 1**, aqueous solutions of calcium nitrate, magnesium nitrate and fuel mixed thoroughly. (A) Citric acid, (B) Succinic acid, (C) Tartaric acid, (D) Sucrose, (E) Urea, (F) Glycine, and (G) L-alanine were used as fuels. Later, TEOS added slowly to the reaction mixture and then nitric acid carefully added. The reaction was continued until the formation of a gel with heating at 70 ^{o}C. Obtained gel was dried in a hot air oven at 70 ^{o}C. Dried gel samples decomposed in a preheated furnace at 400 ^{o}C for 30 min. After decomposition, the precursor obtained found to be in different colors for different fuels. Thus obtained precursor samples calcined at 1300 ^{0}C/ 5h to obtain monticellite. For the phase evolution study, L-alanine assisted precursor compound calcined at different temperatures (600 ^{o}C, 900 ^{o}C & 1300 ^{o}C/ 5h).

2.3 Apatite Formation Ability

All the calcined monticellite powders (prepared by using various fuels) made as compact pellets of 13 mm diameter and 3 mm thickness by using hydraulic pellet press. Similarly, ceramic-polymer composite pellets were also prepared by taking different ceramic to polymer proportions (100, 90:10 and 80:20). L-alanine derived pure monticellite, (chitin and chitosan) biopolymers used to prepare the composites.

2X SBF solution was prepared as per the Kokubo procedure [18, 19]. In brief, all the necessary reagents (NaCl, $NaHCO_3$, KCl, $K_2HPO_4.3H_2O$, $MgCl_2.6H_2O$, HCl, $CaCl_2$, Na_2SO_4, $(CH_2OH)_3CNH_2$) were dissolved in 500 mL of double distilled water one by one at 37 ^{0}C with continuous stirring. After the stepwise dissolution of the reagents, double distilled water again added to increase the total volume of SBF solution to 1 L. Finally, the pH adjusted to 7.4 using a hydrochloric acid solution. The resultant solution filtered and stored in the refrigerator.

Apatite formation ability of monticellite and the composites were investigated by immersing in 2X SBF solution for 10 days and incubated at 37 ^{o}C. After 10 days the pellets were removed from SBF, washed with deionized water and dried at room temperature. The dried pellets were analyzed by using XRD, SEM and EDS techniques to detect hydroxyapatite formation on the immersed pellet surface.

2.4 In-Vitro Biocompatibility Test

Biocompatibility assessment tests (Cell viability and ALP activity) were carried out at PCBS, Puducherry. Cell viability test was performed on monticellite powders by culturing MG 63 cells in contact mode by MTT assay. Cells were placed on 96 well plate for 24 h and then the cells were washed with DMEM. Later, cells were preserved with various concentrations (5, 10, 50, 100 µg/mL) of monticellite and cells without test sample was used as control. The medium was aspirated and incubated with MTT. The medium containing MTT has decanted and DMSO was added. Absorbance was measured at 570 nm and cell viability (%) was estimated.

For the estimation of ALP activity of monticellite, cells were cultured and treated with two different concentrations (5 & 10 µg/ mL) of monticellite and incubated. After incubation (1, 3, 7 days), cell free supernatants were collected and incubated for 30 min in buffer containing p-NPP. ALP activity

was estimated in culture supernatants, by measuring the release of p-nitro phenol spectrophotometrically at 405 nm.

2.5 Characterization Techniques

Bruker D8 advance X-Ray Diffractometer (Germany) was employed for the phase analysis by using Cu Kα, Ni-filtered radiation (wavelength = 1.540600 Å). Shimadzu IR Affinity-1 CE FTIR Spectrophotometer used to record FT-IR spectra of the samples. DLS particle size distribution curves obtained by using Horiba scientific nanopartica nano particle analyzer SZ-100 by dispersing the powder samples in the ethylene glycol medium. Surface morphology and EDS spectrum of the pellet recorded by using EVO 18 Research (Zeiss India).

3. RESULTS AND DISCUSSION

3.1 Sol-Gel Combustion Synthesis

The addition of metal nitrate solution (calcium nitrate and magnesium nitrate) to fuel solution leads to the formation of metal-fuel complex and TEOS upon acid hydrolysis results in the formation of a silanol group along with ethanol. All these complexes help in the formation of polymeric network gel (fuel-Ca-Mg-silanol-ethanol-nitric acid-water) through the sequential steps such as hydrolysis, condensation, polymerization, and gelation. Different polymeric network structures will form depending on the type of fuel used [20]. Type and number of functional groups present on the fuel will affect the various parameters (Thermochemistry, Enthalpy, time duration, type of gases (nitrates, carbonates) evolves, the amount of carbon content and color of the precursor compound) of the combustion reaction through the formation of different polymeric network structures. Thus, different fuels take different time durations to complete the combustion reaction and the color of obtained precursors varies. However, calcination of precursor prepared using various fuels at high temperature (1300 ^{0}C) results in the formation of a white color compound, which may be due to the formation of monticellite. The possible chemical reactions, decomposition and phase evolution studies were shown in the **scheme 1**.

3.2 XRD Analysis

The **Fig. 2** shows the XRD pattern of the precursor sample (L-alanine derived) calcined at different temperatures for phase evolution study. Dual phases corresponding to diopside and merwinite was observed after calcination of monticellite precursor at 600 ^{o}C. The presence of these materials

commonly noticed during the preparation of tertiary system silicates (calcium magnesium silicate) due to non-stoichiometric calcium-rich sites in the heated sample [21]. The absence of monticellite phase in the XRD pattern was due to the lack of optimum temperature required to achieve its crystallization. Hence, to initiate the phase formation of monticellite the precursor was further calcined at a higher temperature. After calcination at 900 ºC, characteristic monticellite peaks emerged as a dominant phase. The diopside and merwinite phases were found to be highly unstable in the temperature range of 700 to 900 ºC, leading to their complete elimination. Moreover, akermanite as a minor phase was also observed along with monticellite at 900 ºC. When the calcination temperature of the sample increased to 1300 ºC, the akermanite phase was found to be completely removed and a single monticellite phasic pure monticellite was obtained. The required temperature for the synthesis of pure monticellite by the sol-gel combustion method was optimized at 1300 ^{0}C. This temperature was found to be very low as compared to existing reports [9, 22]. The XRD pattern of the sample calcined at 1300 ºC was matched with standard JCPDS (Card No: 035-0590) and formation of single phasic monticellite in orthorhombic crystal system with space group Pmnb (62) was confirmed.

The monticellite powders prepared using different fuels were calcined at 1300 ºC and compared XRD pattern shown in **Fig. 3.** It was observed that the XRD patterns were composed of dual phases with the existence of monticellite as well as akermanite peaks. This might be due to the formation of stable akermanite when prepared by citric acid, succinic acid, tartaric acid, sucrose, urea, and glycine as fuels. Hence, it can be suggested that the akermanite phase can be eliminated either by increasing the calcination time or temperature. This finding also indicates that L-alanine is a suitable fuel for the synthesis of pure monticellite.

Table 1 represents the lattice parameters, unit cell volume and crystalline sizes calculated for monticellite samples prepared by using various fuels. The crystallites size was calculated by using Scherer's formula for the highest intense (131) plane. It was found to be in the range of 16-44 nm. The unit cell volume was found to be in the range of 339.44723-342.37023 (Å^3).

3.3 Vibrational Spectra

The internal modes of SiO_4 are almost independent of lattice vibrations in the monticellite crystal structure and these SiO_4 vibrational levels split due to symmetry. Earlier, Handke and Urban determined the splitting modes of the SiO_4 for orthosilicate structures. FT-IR spectra **(Fig. 4.)** of the

precursor calcined at 1300 °C (prepared by using various fuels) shows a sharp band at 826 cm^{-1} which attributed to A_1 (υ_1) stretching mode, the bands appeared at 993, 961, 866 cm^{-1} assigned to the F_2 (υ_3) stretching mode, sharp bands appeared at 601, 516 cm^{-1} assigned to F_2 (υ_4) bending mode and bands appeared at 482,436 cm^{-1} assigned to E(υ_2) bending modes. All the observed vibrational frequencies in good agreement with the Handke and Urban reports [23]. No significant vibrational variations observed in the FT-IR spectra of the monticellite prepared by using various fuels, which indicates the formation of the monticellite phase.

3.4 DLS Analysis

Fig. 5 shows the DLS particle size distribution curves of the monticellite prepared by using various fuels. From the results, it was clear that all the samples in the particle size range of 2162 to 2731 nm. There is no significant variation observed in the particle size distribution of the monticellite prepared by using various fuels.

3.5 Apatite Formation Ability and Biocompatibility

Apatite formation ability of the monticellite pellets (prepared by using various fuels) was tested by immersing in the 2X SBF solution for 10 days (**Fig. 6 (i)**). This was done to analyze the influence of fuels on the apatite formation ability of the monticellite. Urea derived monticellite shows crystalline hydroxyapatite deposition and other fuel derived samples show the amorphous apatite phase. This observation indicates that monticellite samples have the potential to induce apatite formation when exposed to the physiological environment. The rapid exchange of alkaline earth ions from urea derived monticellite samples with H^+ ions from SBF might lead to the formation of the silica-rich layer at a very faster rate. This process resulted in the rapid consumption of Ca^{2+} and P ions from the SBF to initiate hydroxyapatite deposition. Previous studies suggest that the formation of the silica-rich layer at the interface of materials is the major step to induce apatite nucleation [24]. The overall mechanism of apatite deposition is explained elsewhere [25]. The pure monticellite shows improved bioactive within 10 days as compare to earlier reports. Previous articles reveal that the hydroxyapatite deposition on the monticellite surface takes place after immersing in SBF for 15 days [9].

Fig. 6 (ii) shows the XRD pattern of monticellite (L-alanine derived) and its composite pellets after immersing in 2X SBF. After 10 days of immersion, monticellite peaks became less intense and partially disappeared with the appearance of characteristic hydroxyapatite peaks as a major phase. A

comparative apatite deposition behavior of monticellite-chitosan and monticellite-chitin composites were also analyzed. It was found that chitosan favors the deposition of hydroxyapatite whereas chitin was unable to induce hydroxyapatite formation on the surface of composites **Fig. 6 (ii)**. This behavior was found similar to the existing report [26]. This study shows that the content as well as the compositional dependent bioactivity of the samples in a physiological environment. Also, as the chitosan content was decreased in the composites an increase in the rate of apatite deposition was noticed. But the monticellite/chitosan composites did not exhibit better apatite deposition ability than pure monticellite. Hence, this analysis indicates that the bioactivity of ceramics can be influenced by fabricating their composites with biopolymers. A literature survey shows that the monticellite composites are very rarely studied while its composites with biopolymers are still unexplored [27].

Fig. 7 shows the SEM and EDS analysis data of the pure monticellite pellet after immersing in 2X SBF solution. From the SEM images, the morphological appearance of the monticellite pellet surface observed to cover with spherical shaped hydroxyapatite particles, which evenly spread throughout the surface. The appearance of characteristic peaks corresponding to Ca, Mg, Si, O, and P proves the apatite formation ability of monticellite.

Cell viability and ALP tests were performed on MG-63 cell lines for pure Monticellite sample. The test results were shown in **Fig. 8**. An increase in the concentration of the Monticellite sample causes a decrease in cell viability up to 50 ug/mL concentration. In ALP test, we did not find any significant difference by varying incubation time. However, we can see a slight decrease in the ALP activity when the concentration of the sample increased.

4 CONCLUSION

For the first time, monticellite powders were synthesized by employing a sol-gel combustion method and studied the effect of fuel on the phase formation. The methodology used in current work assisted in reducing the calcination temperature of monticellite by ~ 150 ^{o}C. Phase evolution study indicates that the formation of the monticellite from diopside, merwinite, and akermanite. XRD pattern confirms the formation of the pure monticellite phase when L-alanine used as a fuel. In the case of other fuels, the existence of akermanite as a secondary phase observed, which indicates that L-alanine is a suitable fuel for the synthesis of the monticellite phase. Vibrational spectra confirm the presence of monticellite functional groups and DLS data reveals the particle size range from 2162 to 2731 nm.

Apatite formation ability studies show the bioactive characteristics of the pure monticellite within 10 days. Previous reports reveal that the hydroxyapatite deposition on the monticellite surface takes place after immersing in SBF for 15 days. Thus, monticellite may be a potential candidate material for bone regeneration and tissue engineering applications.

ACKNOWLEDGMENTS

Authors acknowledge the support of VIT University and Panjin Institute of Industrial Technology.

REFERENCES

[1] Chen X, Liao X, Huang Z, You P, Chen C, Kang Y, Yin G. Synthesis and characterization of novel multiphase bioactive glass-ceramics in the CaO-MgO-SiO_2 system. Journal of Biomedical Materials Research B: Applied Biomaterials, 2010, 93:194-202.

[2] Nonami T, Tsutsumi S. Study of diopside ceramics for biomaterials. Journal of Material Science: Materials in Medicine, 1999, 10:475–479.

[3] Ou J GF, Yin GF, Zhou DL, Chen XC, Yao YD, Yang WZ, Wu BL, Xue M, Cui J, Zhu HY, Kang YQ. Preparation of merwinite with apatite-formimg ability by sol-gel process. Key Engineering Materials, 2007, 330:67–70.

[4] Sun HL, Wu CT, Dai KR, Chang J, Tang TT, Proliferation and osteoblastic differentiation of human bone marrow derived stromal cells on akermanite-bioactive ceramics. Biomaterials, 2006, 27:5651–5657.

[5] Wu CT, Chang J, Ni SY, Wang JY. In vitro bioactivity of akermanite ceramics. Journal of Biomedical Material Research A, 2006, 76:73–80.

[6] Sharp Z, Hazen R, Finger L. High-pressure crystal chemistry of monticellite CaMgSiO4. American Mineralogist, 1987, 72:748-755.

[7] Bragg WL, Brown GB. Die Struktur des Olivins. Zeitschrift fur Kristallographie, 1926, 63:538-556

[8] Brown GEJr. Crystal chemistry of the olivines. Dissertation for the Doctoral Degree. Virginia: Virginia Polytechnic Institute, Blacksburg, 1970.

[9] Chen X, Ou J, Kang Y, Huang Z, Zhu H, Yin G, Wen H. Synthesis and characteristics of monticellite bioactive ceramic. Journal of Material Science: Materials in Medicine, 2008, 19: 1257-1263.

[10] Sasikumar S, Vijayaraghavan R. Synthesis and characterization of bioceramic calcium phosphates by rapid combustion synthesis. Journal of Materials Science & Technology, 2010, 26: 1114-1118.

[11] Xu L, Srinivasakannan C, Peng J, Zhang L, Zhang D. Synthesis of Cu-CuO nanocomposite in microreactor and its application to photocatalytic degradation. Journal of Alloys and Compounds, 2017, 695: 263-9.

[12] Yang Q, Meng B, Lin Z, Zhu X, Yang F, Wu S. Increased electrical conductivity and the mechanism of samarium-doped ceria/Al2O3 nanocomposite electrolyte. Journal of the American Ceramic Society, 2017, 100: 686-96.

[13] Du F, Zuo X, Yang Q, Yang B, Li G, Ding Z, Wu M, Ma Y, Jin S, Zhu K. Facile assembly of TiO_2 nanospheres/SnO_2 quantum dots composites with excellent photocatalyst activity for the degradation of methyl orange. Ceramics International, 2016, 42: 12778-12782.

[14] Soubbotin K, Zharikov E, Iskhakova L, Lavrishchev S. Growth of single crystals of monticellite CaMgSiO4: Cr from melt by floating zone technique and the study of their composition. Crystallography Reports, 2001, 46: 1030-1038.

[15] Li Y, Wang Y, Xu X, Yu G, Zhang F. Photoluminescence Properties and Valence Stability of Eu in CaMgSiO4. Journal of Electrochemical Society, 2010, 157: J39-J43.

[16] Koppala S, Swamiappan S. Glowing Combustion Synthesis, Characterization, and Toxicity Studies of Na_2CaSiO_4 Powders. Material and Manufacturing Processes, 2015, 30:1476-1481.

[17] Choudhary R, Koppala S, Swamiappan S. Bioactivity studies of calcium magnesium silicate prepared from eggshell waste by sol–gel combustion synthesis. Journal of Asian Ceramic Societies, 2015, 3: 173-177.

[18] Kokubo T, Kushitani H, Sakka S, Kitsugi T, Yamamuro T. Solutions able to reproduce in vivo surface-structure changes in bioactive glass-ceramic A-W3. Journal of Biomedical Materials Research, 1990, 24:721-734.

[19] Cho S B, Nakanishi K, Kokubo T, Soga N, Ohtsuki C, Nakamura T, Kitsugi T, Yamamuro T. Dependence of apatite formation on silica gel on its structure: effect of heat treatment. Journal of American Ceramic Society, 1995, 78:1769-1774.

[20] Sasikumar S, Vijayaraghavan R. Solution combustion synthesis of bioceramic calcium phosphates by single and mixed fuels—A comparative study. Ceramic International, 2008, 34: 1373-1379.

[21] West, A. R. (2003), *Solid State Chemistry and Its Applications*, Wiley.

[22] Chen, X., Ou, J., Wei, Y., Huang, Z., Kang, Y. and Yin, G. (2010), 'Effect of MgO Contents on the Mechanical Properties and Biological Performances of Bioceramics in the MgO-CaO-SiO2 System', *Journal of Materials Science: Materials in Medicine* **21**(5), 1463–1471.

[23] Handke M, Urban M. IR and Raman spectra of alkaline earth metals orthosilicates. Journal of Molecular Structure, 1982, 79:353-356.

[24] Hench, L. L. (1991), 'Bioceramics: From Concept to Clinic', *Journal of the American Ceramic Society* **74**(7), 1487–1510.

[25] Liu, X., Ding, C. and Chu, P.K. (2004), 'Mechanism of apatite formation on wollastonite coatings in simulated body fluids', *Biomaterials* **25**(10), 1755–1761.

[26] Rajan Choudhary, Sivasankar Koppala, Aviral Srivastava, Swamiappan Sasikumar. In-vitro bioactivity of nanocrystalline and bulk larnite/chitosan composites: comparative study. J Sol-Gel Sci Technol (2015) 74:631–640

[27] F. Shamoradi, R. Emadi, H. Ghomi, Fabrication of monticellite-akermanite nanocomposite powder for tissue engineering applications, J. Alloys Compd. 693 (2017) 601-605

Table Captions

Table 1 Lattice parameters and particle sizes of the monticellite prepared by using various fuels (A) Citric acid (B) Succinic acid (C) Tartaric acid (D) Sucrose (E) Urea (F) Glycine (G) L-alanine

Figure Captions

Fig. 1 Synthesis of Monticellite by sol-gel combustion method

Fig. 2 XRD pattern of phase evolution study

Fig. 3 XRD patterns of monticellite prepared by using various fuels (A) Citric acid (B) Succinic acid (C) Tartaric acid (D) Sucrose (E) Urea (F) Glycine (G) L-alanine

Fig. 4 FT-IR spectra of monticellite prepared by using various fuels (A) Citric acid (B) Succinic acid (C) Tartaric acid (D) Sucrose (E) Urea (F) Glycine (G) L-alanine

Fig. 5 DLS curves of monticellite prepared by using various fuels (A) Citric acid (B) Succinic acid (C) Tartaric acid (D) Sucrose (E) Urea (F) Glycine (G) L-alanine

Fig. 6 (i) XRD patterns of monticellite pellets immersed in 2X SBF for 10 days (A) Citric acid (B) Succinic acid (C) Tartaric acid (D) Sucrose (E) Urea (F) Glycine (G) L-alanine **(ii)** XRD patterns of monticellite composite pellets immersed in 2X SBF for 10 days

Fig. 7 Pure monticellite pellet immersed in 2X SBF for 10 days (A) SEM image (B) EDS spectra

Fig. 8 Cell viability (%) and ALP activity of pure Monticellite powders

Schemes

Scheme 1 Reactions involved and phase evolution in the preparation of Monticellite using sol-gel method

Table 1

S. No	Cell Parameters (Å)			Cell Volume (Å^3)	Crystalline Size (nm)
	a	b	c		
Standard	6.366600	11.074100	4.822400	340.000000	-
A	6.37210	11.10683	4.84081	342.60203	25.11
B	6.36011	11.08163	4.81897	339.64287	23.43
C	6.37134	11.10375	4.82477	341.33174	44.32
D	6.36621	11.08795	4.81939	340.19233	44.64
E	6.37103	11.08790	4.82173	340.61353	16.88
F	6.37952	11.10489	4.83274	342.37023	40.10
G	6.35790	11.09052	4.81401	339.44723	34.78

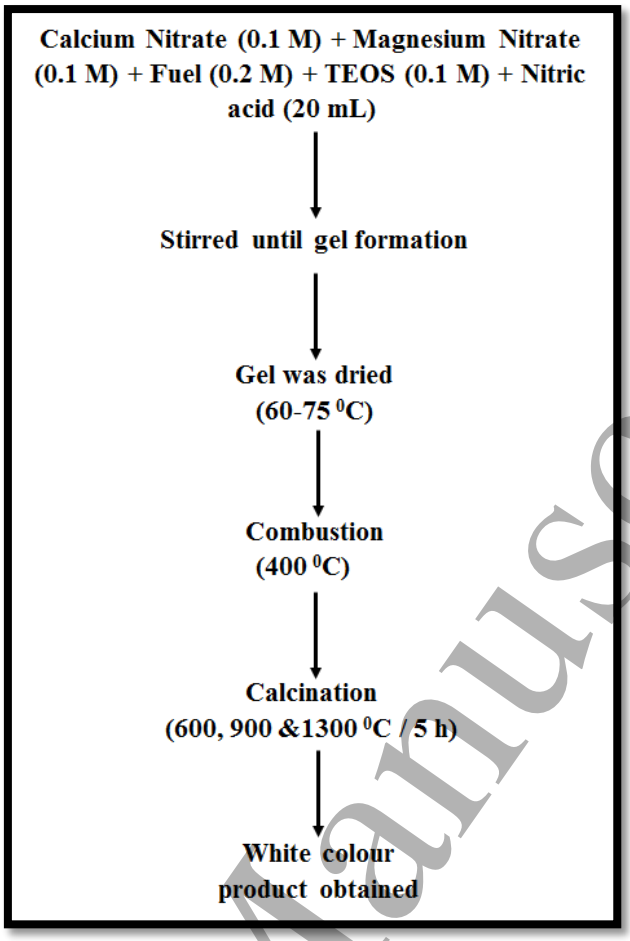

Fig. 1

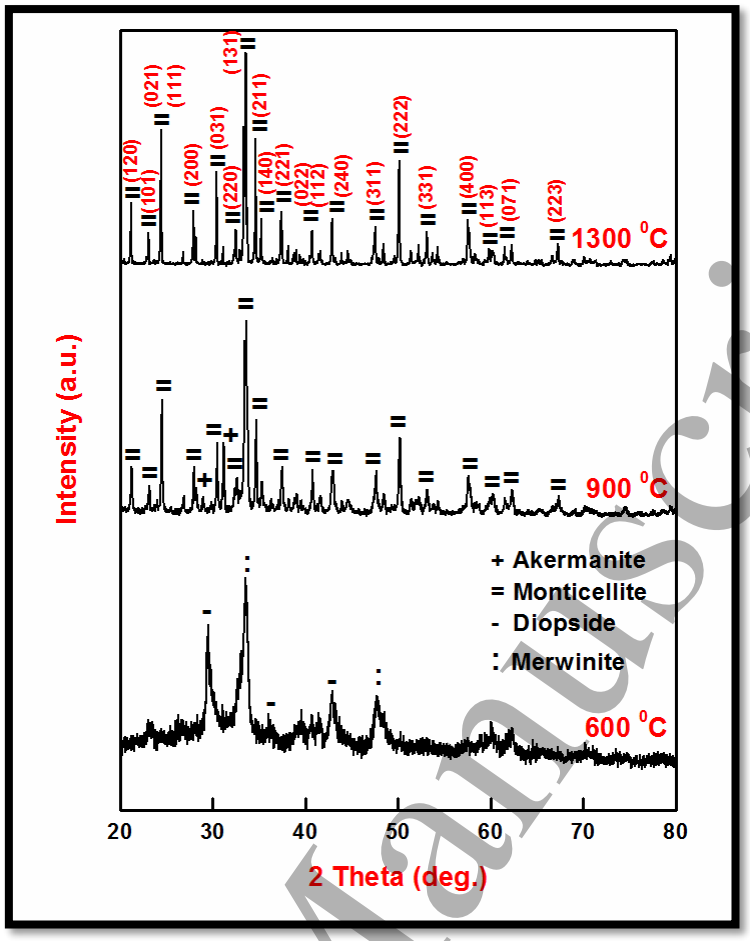

Fig. 2

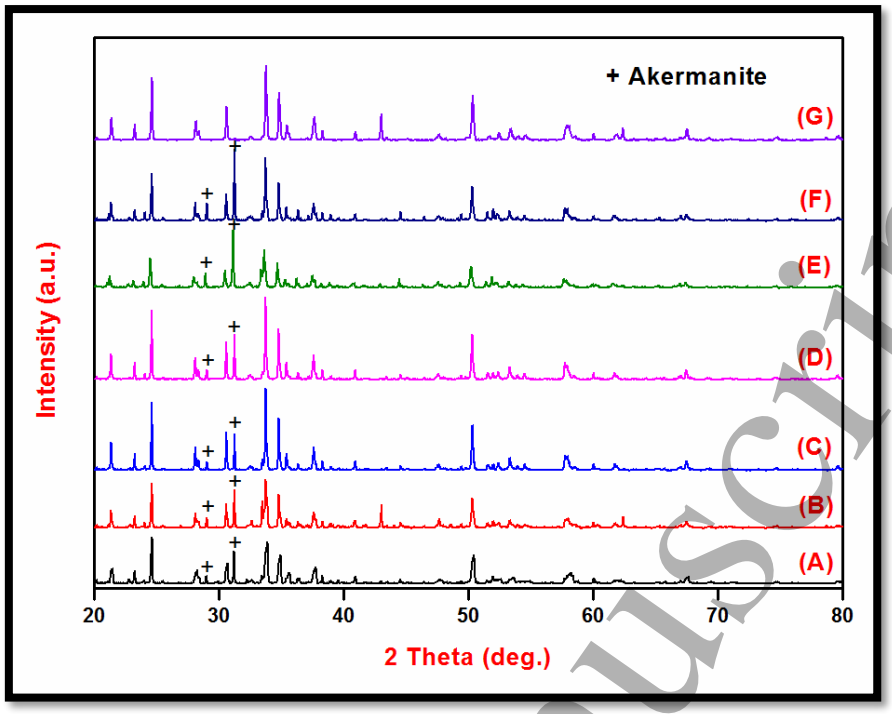

Fig. 3

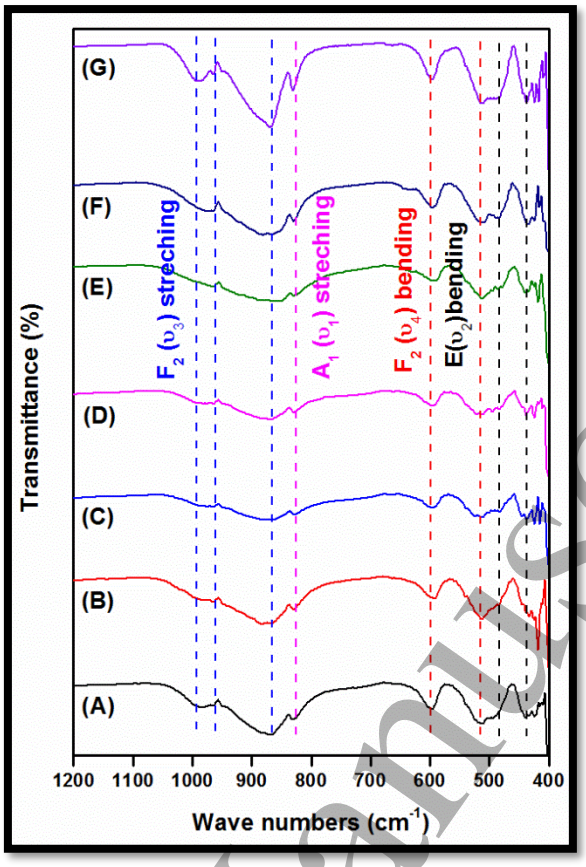

Fig. 4

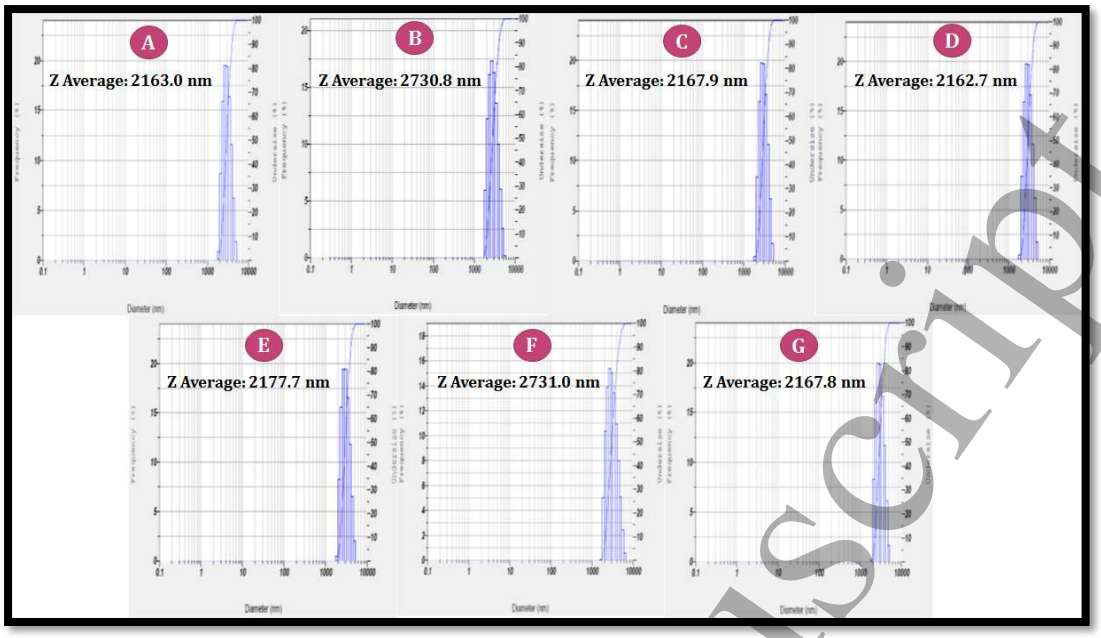

Fig. 5

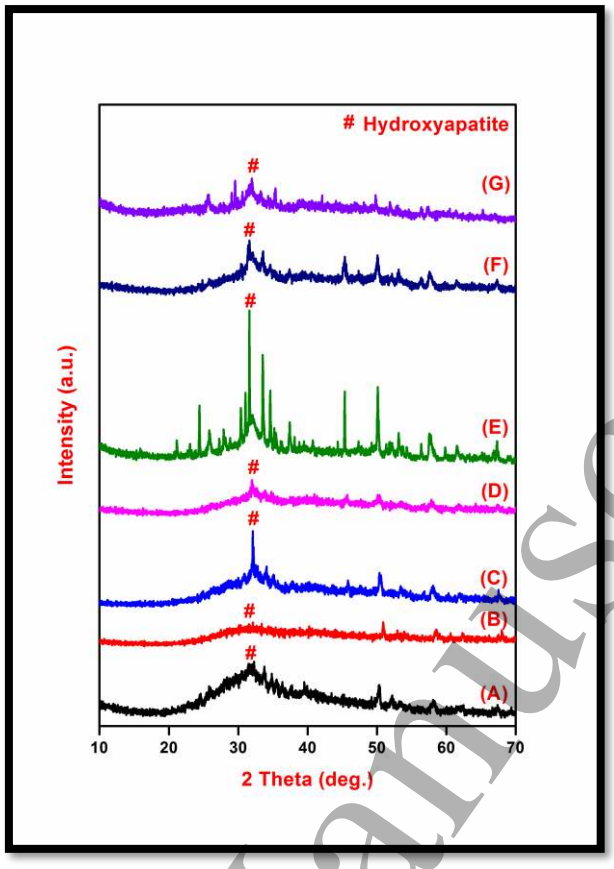

Fig. 6 (i)

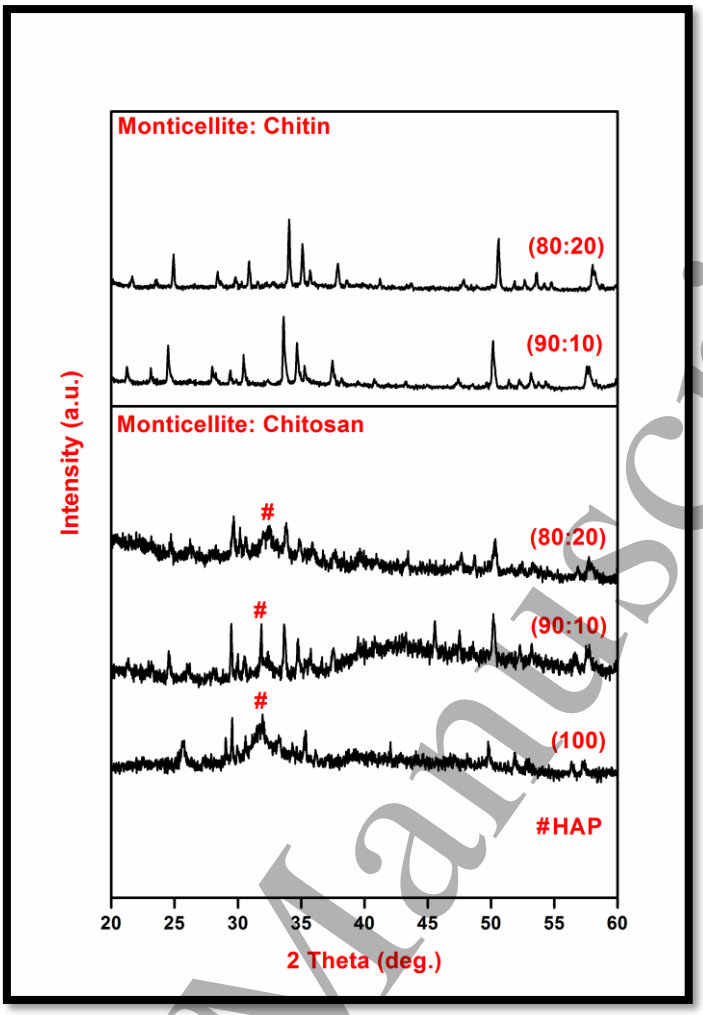

Fig. 6 (ii)

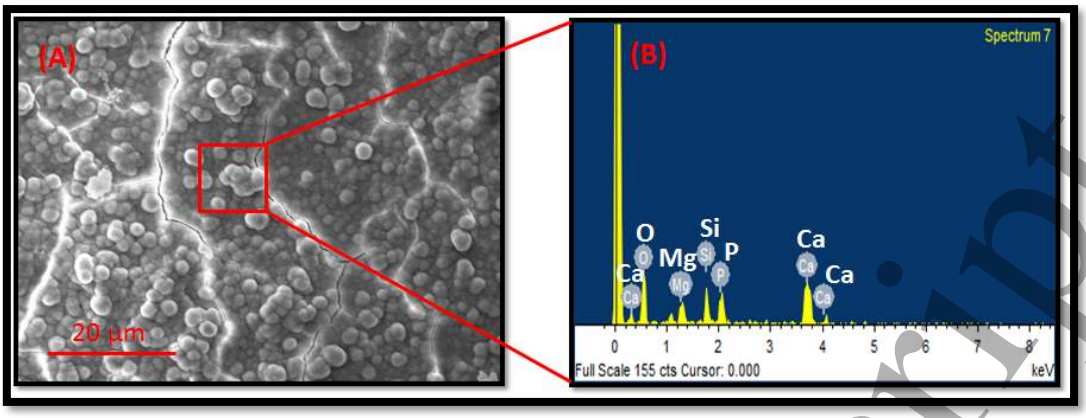

Fig. 7

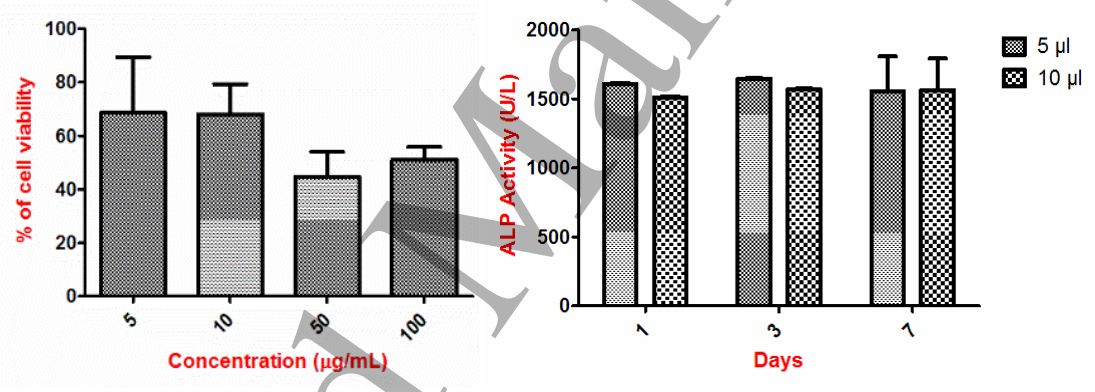

Fig. 8

Scheme 1